Complexity Project
Investigating the Oslo Model's display of Self-Organised Criticality

CID: 01491000

17th February 2022

Abstract: The one-dimensional Oslo Model algorithm was simulated in Python for various sizes with the purpose of investigating the slowly-driven ricepile's tendency to display self-organised criticality. This was demonstrated by proposing finite-size scaling ansatz for the height, height probability and avalanche-size probability, which were then verified through data collapse. The scaling of the height and cross-over time with system size were both theoretically and experimentally demonstrated, with the height probability being inconsistent with a model featuring randomly distributed, independent slopes. Finally the avalanche-size critical exponents were measured to be $D = 2.22 \pm 0.01$, $\tau_s = 1.55 \pm 0.01$ through moment analysis, with corrections to scaling manifesting substantially in the smaller system sizes.

Word count: 2479 words in report (excluding front page, figure captions and bibliography).

Introduction

Self-organised criticality (SOC) refers to the property of slowly-driven non-equilibrium systems with multiple degrees of freedom to self-organise into a highly susceptible state that features scale-free invariance without the external fine-tuning of control parameters. In this project, SOC was investigated by simulating the avalanche dynamics of the slowly-driven one-dimensional ricepile experiment [1] using the Oslo Model. The distinct characteristic of the model is that the threshold slope for a given site is randomly selected to be 1 or 2 every time it relaxes. Despite its simplicity, this feature captures real life spatial and temporal fluctuations and displays SOC in the way that it spontaneously organises itself to a steady state and displays invariant avalanche-size probability.

1 Implementation and Testing of the Oslo Model

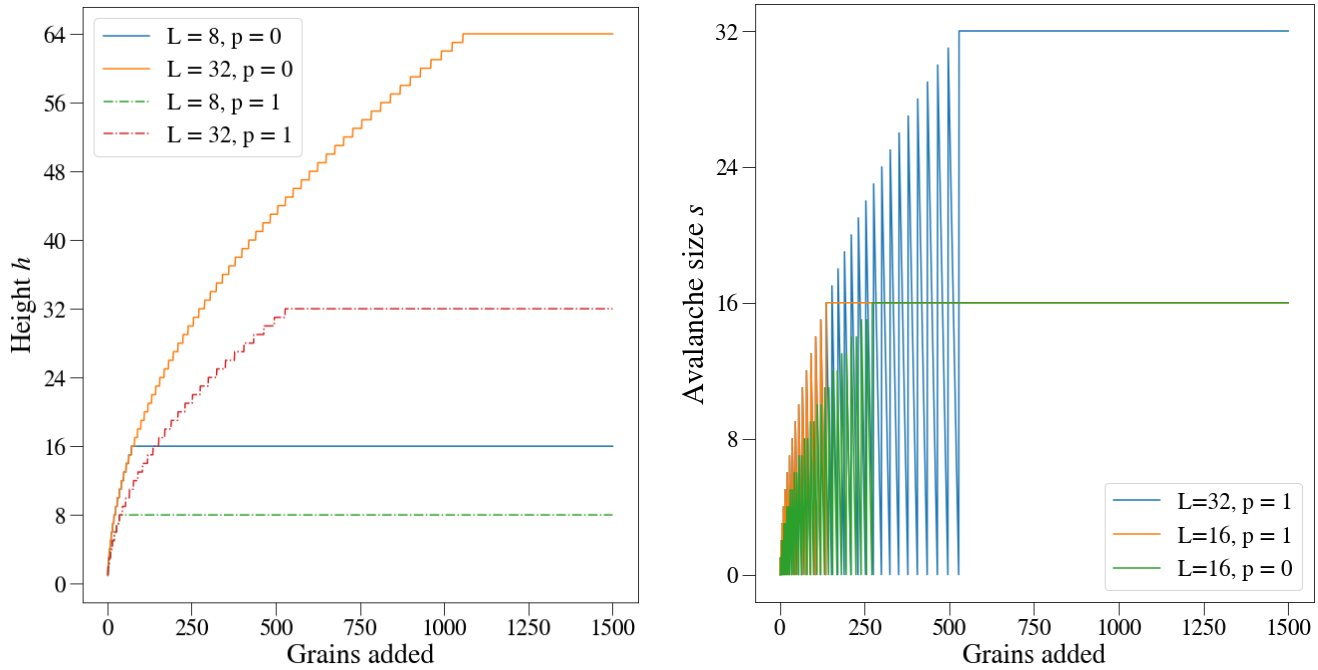

Figure 1: Plots for the tests devised to assess the Oslo model implementation. Fig. 1A: Pile height as a function of grains added. For $p = 0$, the heights reach a constant value at the steady state equal to $h = 16, h = 64$ for $L = 8, L = 32$ respectively. For $p = 1$, the heights reach a constant value at the steady state equal to $h = 8, h = 32$ for $L = 8, L = 32$ respectively. Fig. 1B: Avalanche size plotted against grains added. The avalanche size can be seen to reach a constant equal to the corresponding pile size L for both $p = 0, 1$.

To verify the validity of the algorithm [2], the model was tested on various situations in which the result is known. Namely, by setting $p = 1$ or $p = 0$, all the thresholds during the steady state are expected to be equal to $z_i^{th} = 1$ and $z_i^{th} = 2$ respectively. The height of a pile is given by

$$h(t; L) = \sum_{i=1}^{L} z_i(t) \tag{1}$$

where L is the length of the pile [2]. We thus expect the steady-state height to be constant as $h_{steady}^{p=0} = L$, $h_{steady}^{p=1} = 2L$. Since all the thresholds are equal and non-changing, the steady state

will be reached after adding a number of grains $N^{p=0} = \sum_{i=1}^{L} i = L^2$ and $N^{p=1} = \sum_{i=1}^{L} 2i = L^2/2$ according to their series expansion. It is also expected that the avalanche size s will reach a constant equal to $s_{steady}^{p=0,1} = L$ for both $p = 0, 1$, as the input grains will topple through all sites without inducing relaxations. Figure 1 shows that the implementation is producing the expected behaviour.

The average height in the steady state was then measured with $p = 1/2$ for $L = 16, 32$. The algorithm gave a value of 26.50 ± 0.01 for $L = 16$ and 53.91 ± 0.02 for $L = 32$ for 10^5 grains in the steady state, matching the known accepted values of 26.5 and 53.9 within their standard deviation.

2 Height of the Pile

2.1 Transient and Recurrent configurations

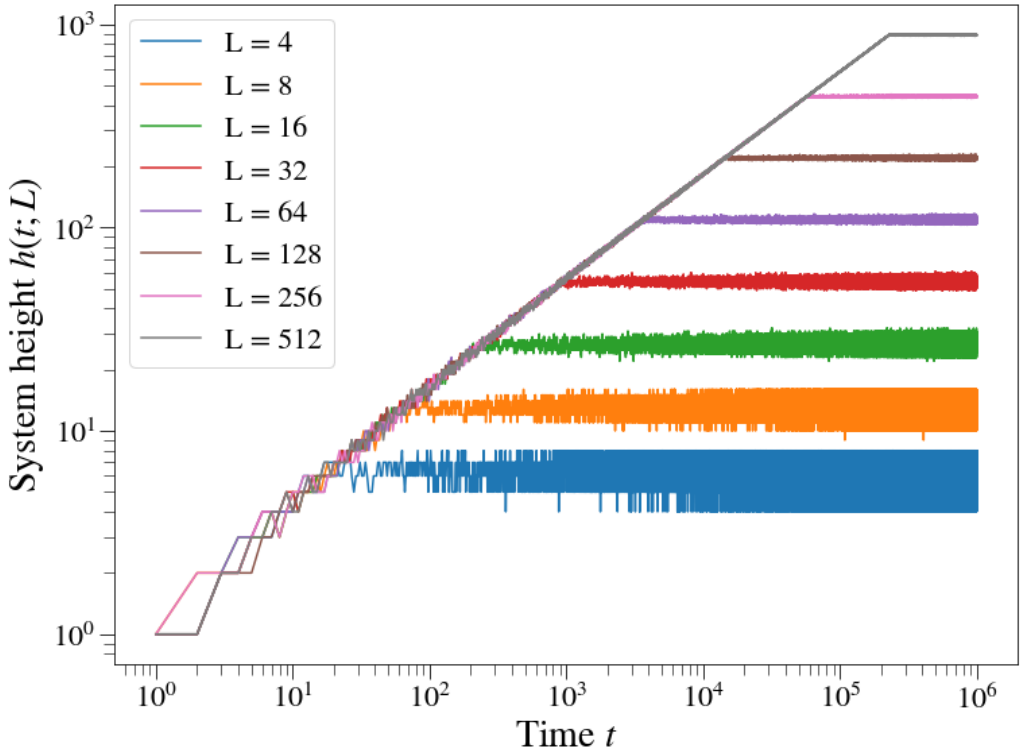

Figure 2: Pile heights $h(t; L)$ against time t for system sizes $L \in \{4, 8, 16, 32, 64, 128, 256\}$. The plot has a log-scale on both axis and is driven for 1.0×10^6 added grains. Before the crossover time t_c, the systems display transient configurations which follow a common power-law relation. After t_c the heights are seen to plateau and fluctuate around a constant steady height which increases with L.

In the Oslo model, a system of finite size L will have a finite set of possible stable configurations, their total being $N_s = 3^L$ [3]. At each induced relaxation, the system rearranges itself to one of the configurations in the stable set. As the system evolves, it first exhibits a period of configurations that appear once (transient) before entering a steady state at a characteristic time t_c which increases with L, where it self-organises to a set of $\mathcal{R}$ recurrent configurations. At that point the height fluctuates around a constant value which depends on L. This behaviour can be seen in Figure 2. As during the transient phase no grains have left the system, the transient configurations of a given system are a subset of the transient configurations of a larger system.

2.2 System Cross-over Time

For a system of size L, the cross-over time t_c is defined as the number of grains in the system before an added grain induces a grain to leave the system for the first time [3].

Measuring Average Cross-over Time

To measure t_c, the pile was driven until the number of grains on the pile did not match the total number of grains added. This indicated that a grain has left the system, with t_c being the exact time before this condition was met. The procedure was repeated was repeated 10 times for system sizes $L \in \{4, 8, 16, 32, 64, 128, 256, 512\}$, with the average $\langle \tau_c \rangle$ and standard deviation σ_{t_c} of each size recorded.

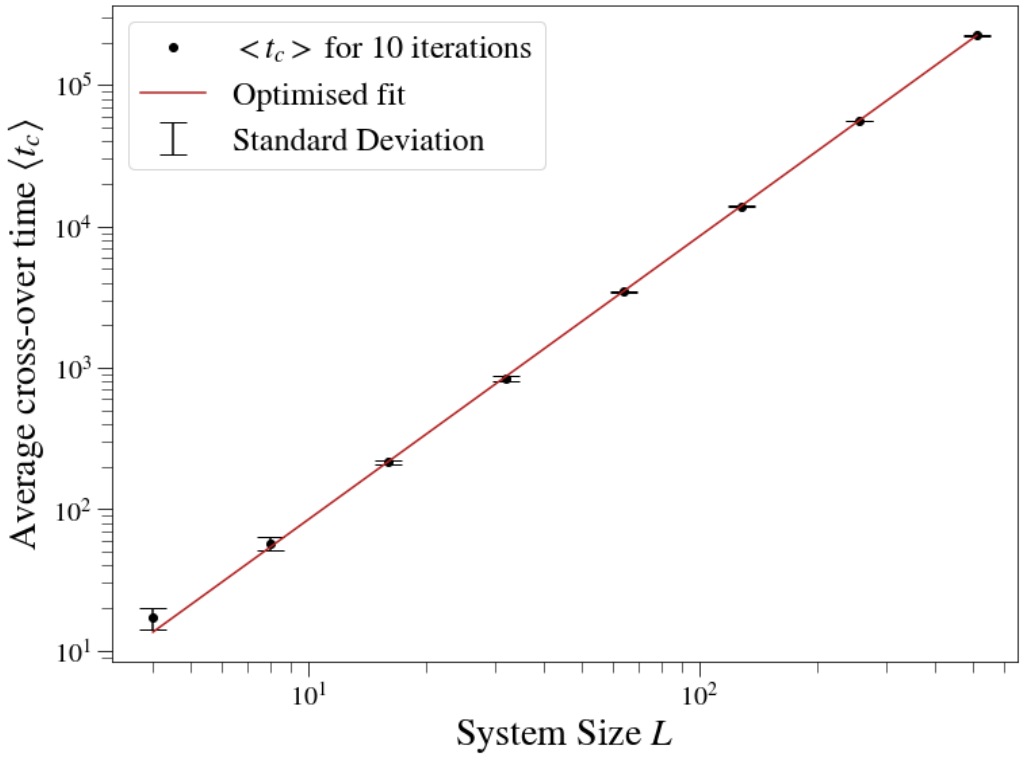

Figure 3: Plot of Average cross-over time $\langle \tau_c \rangle$ against $L \in \{4, 8, 16, 32, 64, 128, 256, 512\}$, averaged over 10 iterations for each system size. The plot has a log-scale on both axis, the black points indicate data points are fitted with error bars corresponding to the standard deviation over the 10 iterations. The red straight line is the optimised power-law fit obtained.

Fitting a power-law relation through the data points for $L \in \{64, 128, 256, 512\}$ yielded the scaling relation of

$$\langle \tau_c \rangle = L^{2.00 \pm 0.01} \tag{2}$$

for $L \gg 1$. The data points for smaller system sizes were ignored as they are susceptible to large corrections to scaling.

Theoretical expectation of the scaling of h and τ_c with L

It was established that the height of the pile in the steady state can be calculated by summing the site thresholds as in equation 1. For $L \gg 1$ and ignoring potential corrections to scaling, the average slope $\langle z \rangle = \frac{1}{L} \sum_{i=1}^{L} z_i$ can be considered a constant independant of L. Thus $h = \langle z \rangle L$, showing that $h \propto L$, with $\langle z \rangle$ being the constant of proportionality.

During the steady state, the pile is roughly shaped as a right-angled triangle for $L \gg 1$. The base has length L and height $h \propto L$. In the steady state the system is past its cross-over time t_c. The number of grains entering the system are equal to the number of grains leaving the system at any time interval, thus area of the triangle Δ_{Area} is proportional to the number of grains added N just before the steady state which is t_c. Therefore $t_c \propto \Delta_{Area} \propto L^2$, which is in agreement to the measured scaling obtain in equation 2.

2.3 Processed Heights and Data Collapse

To produce a data collapse that spanned both the transient and attractor region of the heights, the model was driven for $N = 2L^2$ grains for each size $L \in \{4, 6, 16, 32, 64, 128, 256, 312\}$. The chosen N ensured the system was driven well into its steady state without excessive addition of grains. To reduce noise in height data, the average over M different realisations of the pile for each L were considered, defined by

$$\tilde{h}(t; L) = \frac{1}{M} \sum_{j=1}^{M} h^j(t; L)$$

where $h^j(t; L)$ is the height at time t and jth realisation of a system of size L, and $\tilde{h}$ are the processed heights. Larger Ms were chosen for the smaller heights as they are most susceptible to corrections to scaling.

The time evolution of the system is characterised the cutoff between the scale-free transient states to the recurrent states given by the cross-over time $t_c \propto L^2$. Therefore, guided by the arguments laid in the previous section, dividing the processed heights by L and the time-values by L^2 will cause the data to collapse onto a single scaling function $\mathcal{F}$. On this basis the following finite-size scaling ansatz FSS was proposed:

$$\tilde{h}(t; L) = L\mathcal{F}(\frac{t}{L^2}) \tag{3}$$

By recasting equation 3 in the form $\frac{\tilde{h}(t;L)}{L} = \mathcal{F}(\frac{t}{L^2})$, it can be seen that a plot of $\frac{\tilde{h}}{L}$ against $\frac{t}{L^2}$ will trace out the form of the scaling function $\mathcal{F}$, as depicted in figure 4. The larger system converge convincingly onto a single common FSS, verifying the validity of the proposal in (3).

From the figure it can be observed that for $\frac{t}{L^2} \gg 1$ the scaling function is constant, while for $\frac{t}{L^2} \ll 1$ it follows some power-law relation. This must be the case as it was established that the transient states of a system are indistinguishable to the transient states of a larger system and thus do not scale with L. For $\frac{t}{L^2} \ll 1$, $\mathcal{F}$ must be proportional to $1/L$. For $\frac{t}{L^2} \gg 1$, it was established that $h \propto L$, thus $\mathcal{F}$ must be a constant. Hence the scaling function traced out in 4 is consistent with the form

$$\mathcal{F}\left(\frac{t}{t_c}\right) \propto \begin{cases} \sqrt{\frac{t}{L^2}}, & \frac{t}{L^2} \ll 1 \\ constant, & \frac{t}{L^2} \gg 1 \end{cases}$$

Substituting $\mathcal{F}$ into ansatz (3) for the transient state yields the scaling of the height as

$$\tilde{h}(t; L) \propto L\sqrt{\frac{t}{L^2}} \propto \sqrt{t}$$

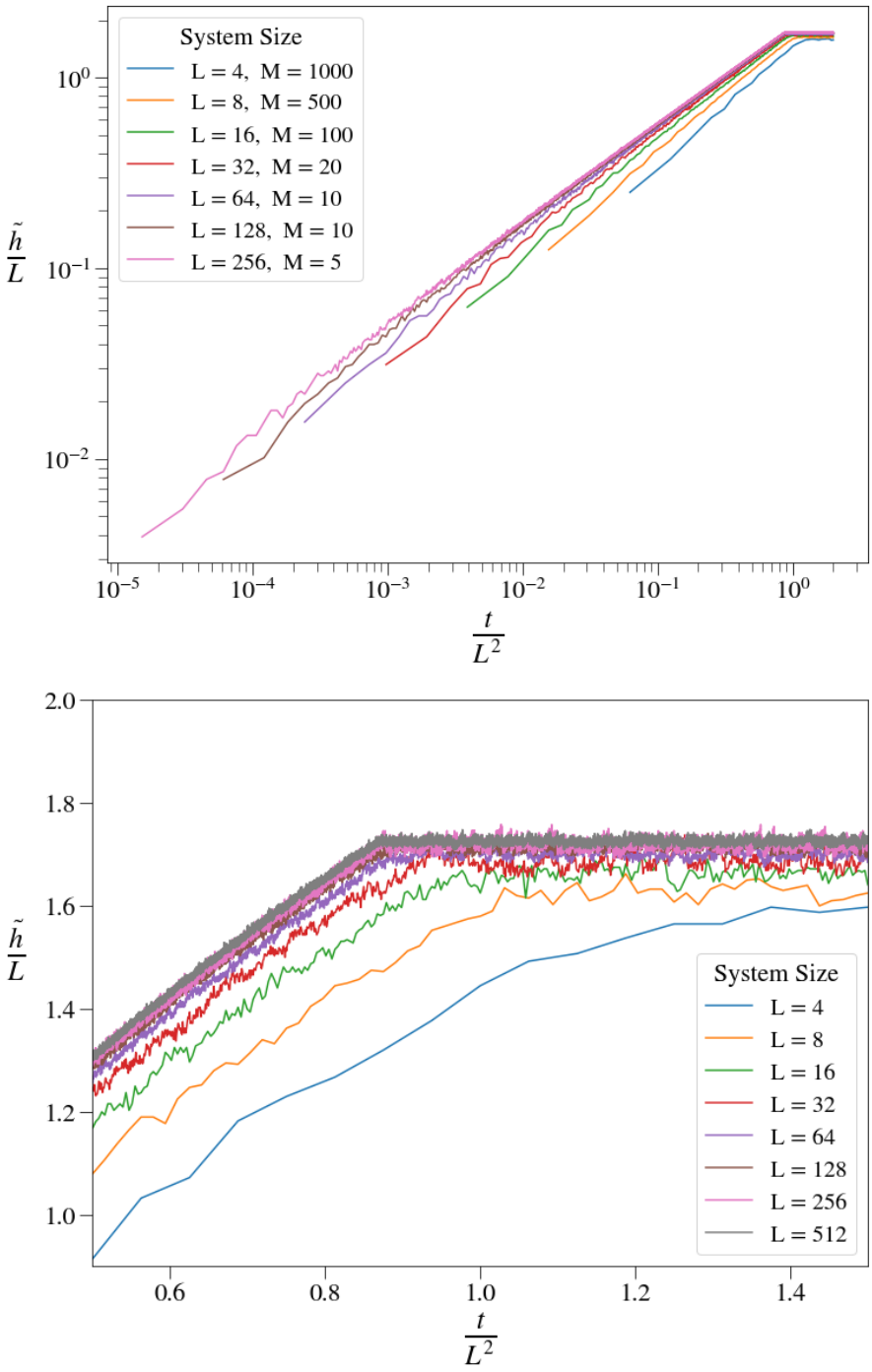

Figure 4: Top: Log-log plot of scaled processed height $\frac{\tilde{h}}{L}$ against scaled time $\frac{t}{L^2}$. The legend displays the system size for each colored line along with the corresponding number of realisations M. The tracing of the scaling function $\mathcal{F}$ is better for larger system sizes which are in closer agreement, hinting at correction to scaling affecting the smaller sizes. The initial rising region is the transient while the constant region after the turning point is the attractor of the system. Bottom: A zoomed in version with normal axes to closer reveal the turning point of the scaling function. Again the larger system sizes have a sharper cut-off than the smaller ones.

Similarly, fitting the transient state of $L = 256$ with a power-law relation, depicted in figure 5, yielding the result $\tilde{h}_{L=256} = L^{0.51\pm0.005}$.

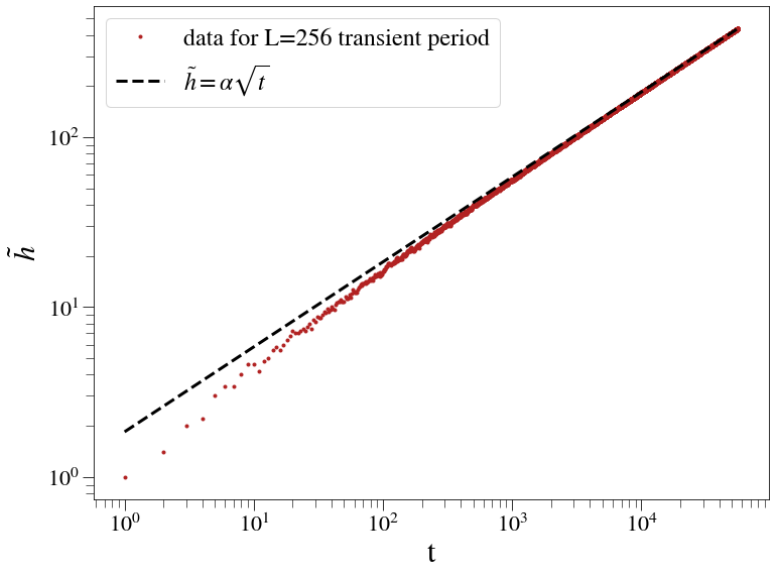

Figure 5: Loglog plot of processed height $\tilde{h}$ against time t for $L = 256$ in the transient phase. The data is fitted with the transient height relation obtained. The fit is in agreement with the data as most of it skewed to the higher height values, a is a constant of proportionality.

2.4 Corrections to Scaling of Processed Heights

In this section, the average height over a time period T of a system size L during steady state was determined using:

$$\langle h(t;L)\rangle_t = \lim_T \frac{1}{T} \sum_{t=t_0+1}^{t_0+T} h(t;L)$$

where t_0 was chosen to be L^2, the upper bound of $t_c(L)$ for each system, and $T = 1 \times 10^6$. This ensured a high enough time period, minimising the standard deviation.

If h scaled exactly linearly with L, plotting $\frac{\langle h\rangle}{L}$ against L should give a straight horizontal line at exactly a_0. This is not the case however as seen in figure 6.

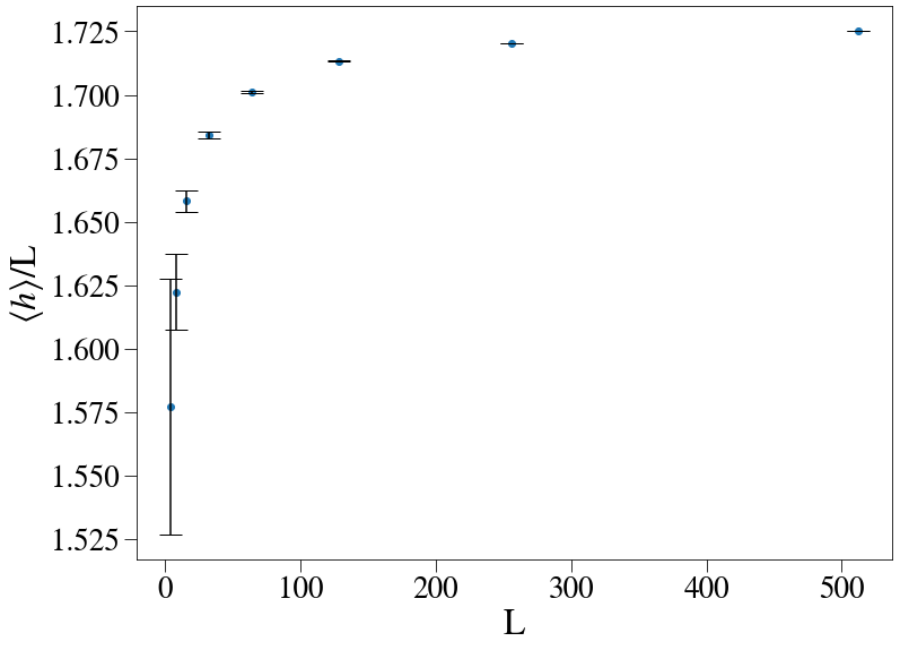

Figure 6: Plot of $\frac{h}{L}$ against L. The result it not a straight line, implying that corrections to scaling are at play, especially affecting the lower system sizes.

Corrections to scaling of the average steady state height were introduced in the form:

$$\langle h(t;L)\rangle_t = a_0 L\left(1 - a_1 L^{-\omega_1} + a_2 L^{-\omega_2} + \ldots\right)$$

where a_i and $\omega_i > 0$ are constants. Neglecting terms of order higher than 1 results in:

$$\langle h(t;L)\rangle_t = a_0 L(1 - a_1 L^{-\omega_1}) \tag{4}$$

To obtain a_0 and ω_1 equation 4 was recast as:

$$\log\left(1 - \frac{\langle h(t;L)\rangle_t}{a_0 L}\right) = -\omega_1 \log L + \log a_1$$

A plot of the left-hand-side as a function of $log(L)$ with the correct value of a_0 produces a straight line with a gradient of $-\omega_1$ as seen in figure 7. The straight line was obtained by manually tuning the values of a_0 until a straight line was traced, resulting in the result $a_0 = 1.74 \pm 0.01$. A linear curve-fit yielded a gradient value of $\omega_1 = 0.51 \pm 0.01$.

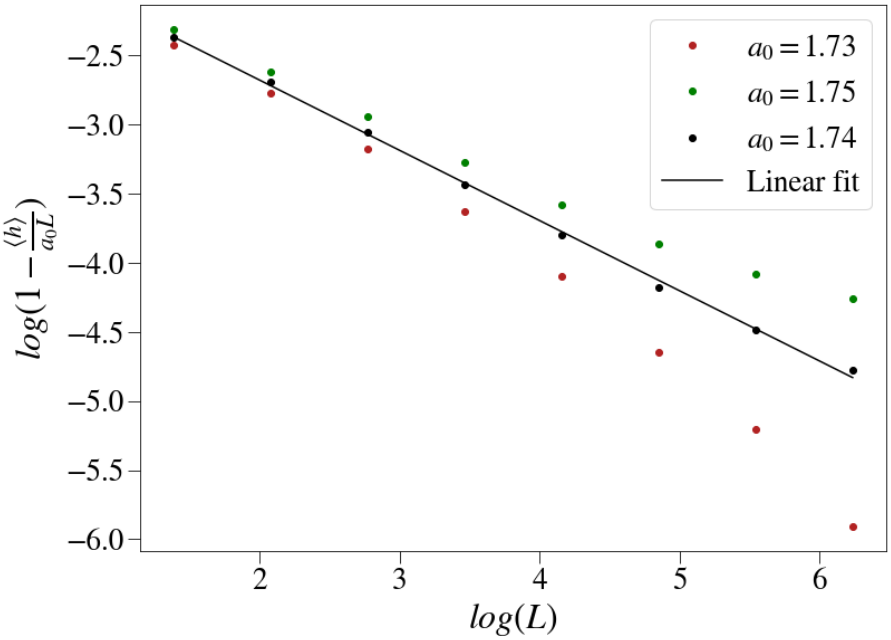

Figure 7: Plot of left-hand-side of equation 4 against $\log L$. It can be seen that a deviation of 0.01 to the value of $a_0 = 1.74$ results in non-straight lines. The black line is the linear curve-fit obtained, which has gradient $-\omega_1$.

When compared to directly curve-fitting equation 4, this procedure reduces the number of parameters to be fitted from 3 to 2. As a result the value of ω_1 is less prone to deviations due to a change in a single data point.

2.5 Standard deviation of Heights and Average Slopes

The standard deviation of the height for each system size, calculated using

$$\sigma_h(L) = \sqrt{\langle h^2(t;L)\rangle_t - \langle h(t;L)\rangle_t^2}$$

was plotted against L, depicted in figure 8, and fitted with a power-law. The scaling behaviour was found to be $\sigma_h \propto L^{0.24\pm0.01}$, with the error of the exponent obtained through the covariance matrix of the fit. The 0.58 in the fit is a constant of proportionality.

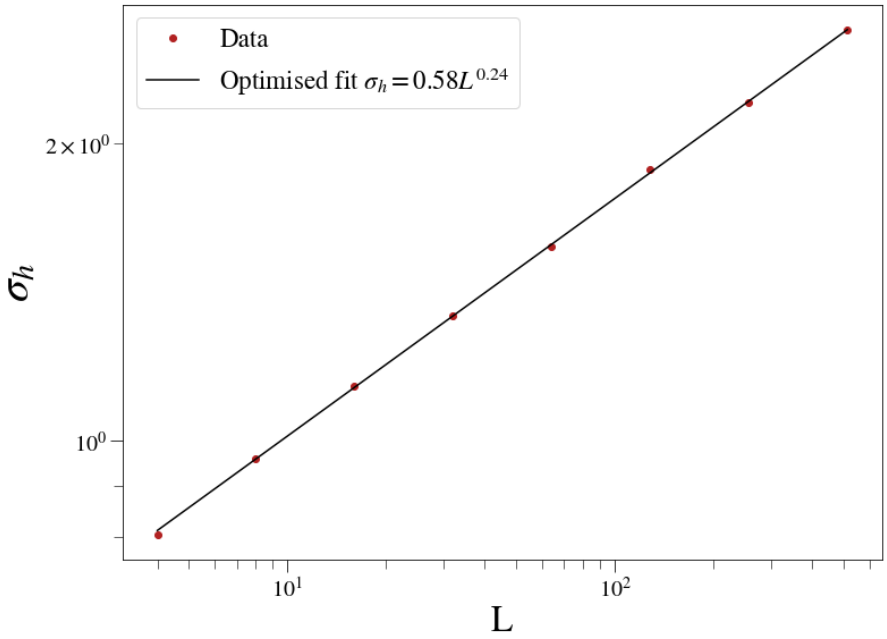

Figure 8: Log-log plot of standard deviation of the height σ_h against system size L. The black line is the optimised fit obtained through linear fitting, while the red dots are the data points.

We have established in section 2.2 that that the height of the pile in $L \gg 1$ can be obtained by $h = \langle z \rangle L$, and thus the average slope $\langle z \rangle = \frac{\langle h \rangle}{L}$. Therefore the standard deviation of the average slope $\sigma_{\langle z \rangle} = \frac{\sigma_h}{L} \propto L^{-0.76}$, and thus would tend to 0 as $L \to \infty$. Furthermore, taking into account the corrections to scaling relationship equation 4, the average slope would follow

$$\langle z \rangle = \frac{\langle h \rangle}{L} = 1.74(1 - a_1 L^{-0.51})$$

which tends to the constant $a_0 = 1.74$ as $L \to \infty$.

2.6 Height Probability

Considering the pile height as defined in equation 1, if the slopes at each site z_i are assumed to be independent, identically distributed random variables with finite variance, then the height probability for a given L is expected to tend towards a gaussian distribution as L gets larger. This is according to the Central Limit Theorem [4], which states that the distribution of the sum of random variables approximates a normal distribution for large sample sizes. Specifically, for the random variable z_i which follows a distribution with mean $\langle z \rangle$ and standard deviation σ_z, the resulting summation $h = \sum_{i=1}^{L} z_i$ will be gaussian with mean $\mu = \langle h \rangle = L\langle z \rangle$ and standard deviation $\sigma_h = \sigma_z \sqrt{L}$, expressed mathematically as:

$$P(h; L) \propto \frac{1}{\sigma_h} \exp\left(-\frac{1}{2}\left(\frac{h - \langle h \rangle}{\sigma_h}\right)^2\right) \tag{5}$$

Using the height data displayed in section 1, the measured height probability $P(h; L)$ for each L was calculated and is plotted in figure 9.

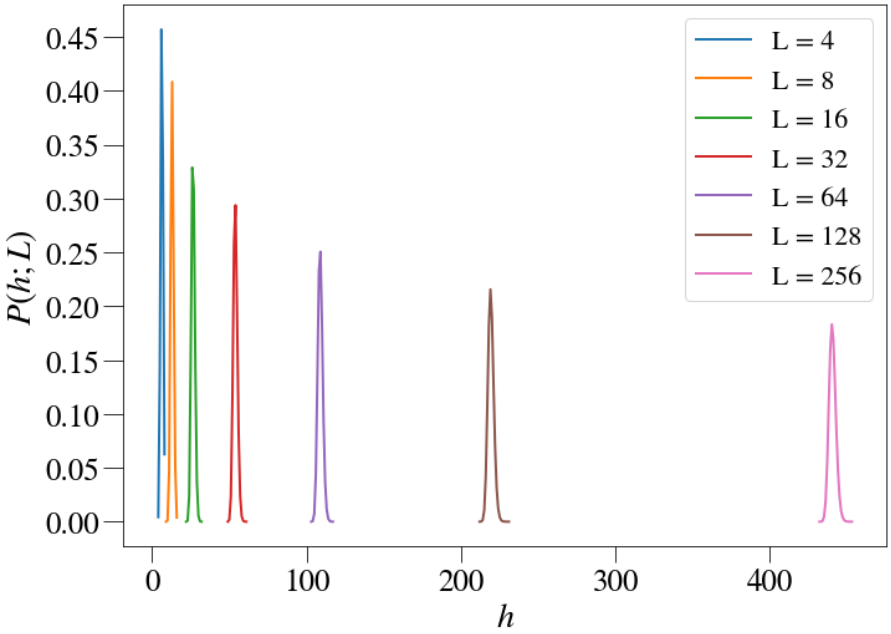

Figure 9: Measured height probability $P(h; L)$ against height h. The distributions for each height appear to follow a Gaussian shape, with peaks at the average heights $\langle h \rangle$ as calculated in section 2.4. Here the probability for $L = 512$ was omitted to make the smaller size probabilities more visible.

Following the formulation of the distribution in equation 5, a data collapse of the probabilities can be produced by rescaling the probabities as $\sigma_h P(h; L)$ and plotting it against $\frac{h-\langle h \rangle}{\sigma_h}$. This would trace out the scaling function $\mathcal{G}(x) = \exp -\frac{1}{2}x^2$ where $x = \frac{h-\langle h \rangle}{\sigma_h}$ with $\mu = 0$ and $\sigma = 1$. Figure 10 depicts the probability data collapse for the measured height probabilities, with their corresponding standard deviations σ_h used for the scaling.

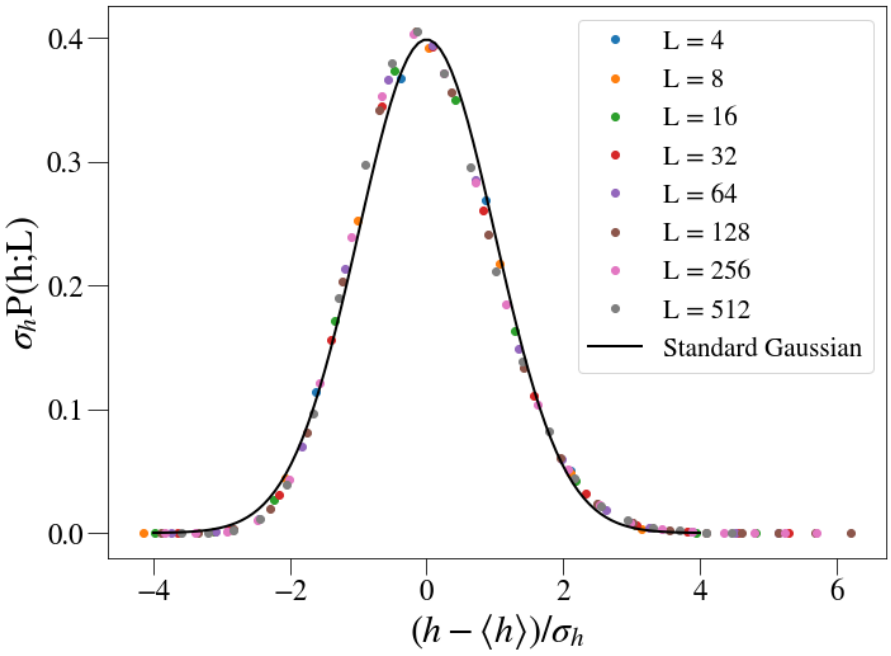

Figure 10: Plot of scaled height probability against scaled height, producing a data collapse. The data points for various pile sizes is depicted and labelled in the figure legend, along with a standard gaussian centred at 0 with standard deviation set to 1. The tail-end of the data is longer and the peak does not match the standard gaussian expectation but rather seems to skew to the right.

Judging from the figure, the data points measured disagree with the expected Gaussian distribution ansatz. This implies that the slopes z_i cannot be assumed to be independent variables. For one, $z_i = 2$ is more stable and thus more probable in a given recurrent configuration than $z_i = 1$. This is because $z = 1$ is more likely to exceed its threshold and relax, resetting its threshold to an equally likely 1 or 2. Thus the thresholds are not independent. Running a simple test of measuring the average slope over a time period $T = 1 \times 10^6$ yielded the resulting $\langle z_i \rangle = 1.74 \pm 0.01$, which does not match the expected 0.5 value were the two thresholds equally probable. This might be the reason of the skeweness of the Gaussian, as a few higher height values would move the mean, but not the median, of the distribution to the right.

To test whether the traced out function is indeed not a Gaussian, the data for large L can be fitted and numerically integrated from $-\infty$ to 0 and from 0 to $+\infty$. If these do not match, then the traced function is indeed not Gaussian. Another test that could be conducted is running the Oslo model without the imposing a new threshold probability at each relaxation. This effectively makes the (permanent) thresholds random variables, and the same collapse should trace Gaussian ansatz.

3 Avalanche-Size

An avalanche size s is defined as the sum of relaxations caused by an addition of a single grain at site $i = 1$. This includes avalanches of size $s = 0$ for the purpose of a correct normalisation. The avalanche size probability follows a power-law distribution. As a result, the raw output of the data suffers from substantial noise towards the tail end of the distribution, owing to the insufficient statistics to trace out the underlying probability distribution for large s and the finite-size effects of large systems.

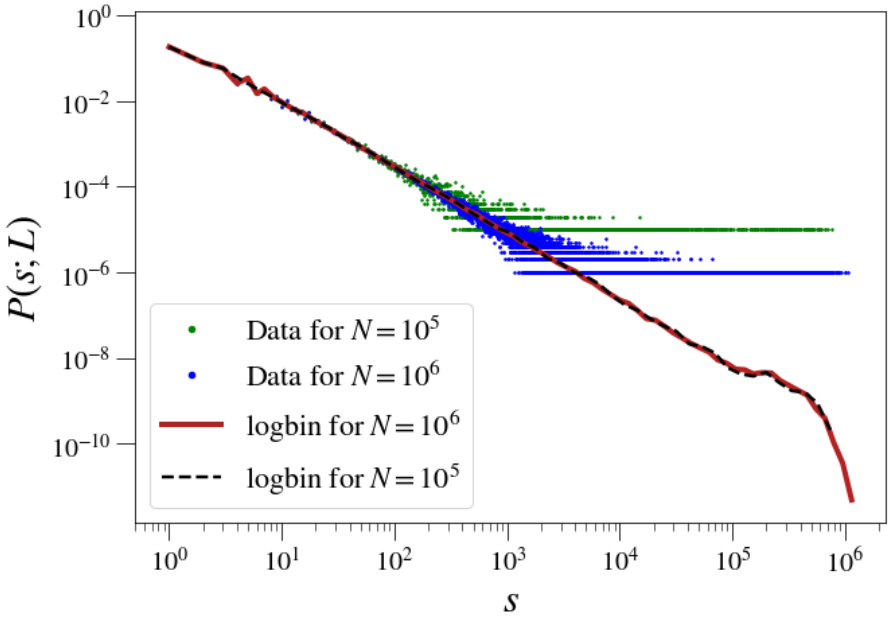

Figure 11: Plot of raw avalanche-size probability $P(s;L)$ against avalanche size s for $L = 512$ (dots) for total number of avalanches $N = 10^5$ and $N = 10^6$. The log-binned probability $\tilde{P}(s;L)$ for both data sets is also plotted (lines). The cutoff in the log-binned data is more visible for the larger N, which was chosen for the following considerations.

To overcome this limitation, a logarithmic binning procedure [3] is applied, in which the data is grouped into bins with exponenially increasing sizes. Samples of varying sizes N were tested,

some examples shown in figure 11, with $N = 10^6$ determined to be sufficiently large to expose the tail cutoff. The data was tested with growth factor values a between each consecutive bin 1.0 to 2.0 in steps of 0.1, with $a = 1.2$ producing the more visually suitable results. This is depicted in figure 12.

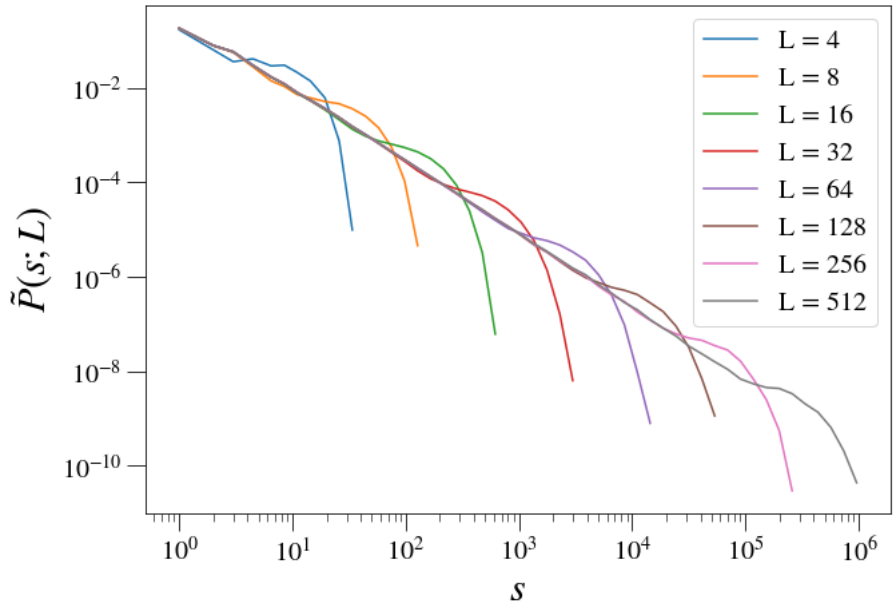

Figure 12: Log-log plot of Log-binned avalanche-size probability $\tilde{P}(s;L)$ against s for system sizes $L \in \{4, 8, 16, 32, 64, 128, 256, 512\}$. There is a clear pattern of behaviour that is obeyed by all system sizes, namely a power-law region, followed by a characteristic 'upper bump', and then a decrease. Avalanche sizes span several orders of magnitude, reaching much higher sizes than their system size despite the input drive being the addition of a single grain.

From the figure, it can be seen that the graphs have some general features that are universal across all L. All system size graphs feature a common linear decay region in the log-plot, followed by a pronounced bump and a cut-off at $s = s_c$ where $\tilde{P}(s;L)$ rapidly decreases to 0. In the region well before the characteristic cutoff $1 \ll s \ll s_c(L)$, the probability $\tilde{P}(s;L)$ is seen to be scale invariant and follow a power-law decay, thus $\tilde{P}(s;L) \propto s^{-\tau_s}$, where t_s is the avalanche size exponent. No typical avalanche size can be seen other than s_c which increases with system size L, implying that $s_c \propto L^D$ where D is the avalanche dimension.

For any given system, it can be seen that a single grain can cause avalanches with sizes spanning several orders of magnitude. The response of the pile in the steady state to the addition of a grain is highly non-linear and scale-free, therefore displaying SOC.

3.1 Scaling ansatz

Following the analysis in the previous section, a finite-size scaling ansatz for $L \gg 1$,$s \gg 1$ can be introduced as

$$\begin{aligned} \tilde{P}_N(s;L) &\propto s^{-\tau_s}\mathcal{G}\left(s/s_c\right) \\ s_c &\propto L^D \end{aligned} \tag{6}$$

Is important to note that D and t_s are finite size exponents and thereby subject to corrections to scaling. By recasting the ansatz in the form

$$s^{\tau_s}\tilde{P}_N(s;L) \propto \mathcal{G}\left(\frac{s}{L^D}\right)$$

it is then clear that τ_s re-scales the y-axis and can align the distinct feature of each graph horizontally, while D rescales the x-axis and aligns the data vertically. The ansatz can then be verified based on the agreement of a data collapse.

To estimate τ_s the intermediate section $1 \ll s \ll s_c$ of $\tilde{P}(s, L = 512)$ was fitted with a power-law (figure 13), yielding $\tau_s = 1.55 \pm 0.01$, error obtained from the fit covariance matrix.

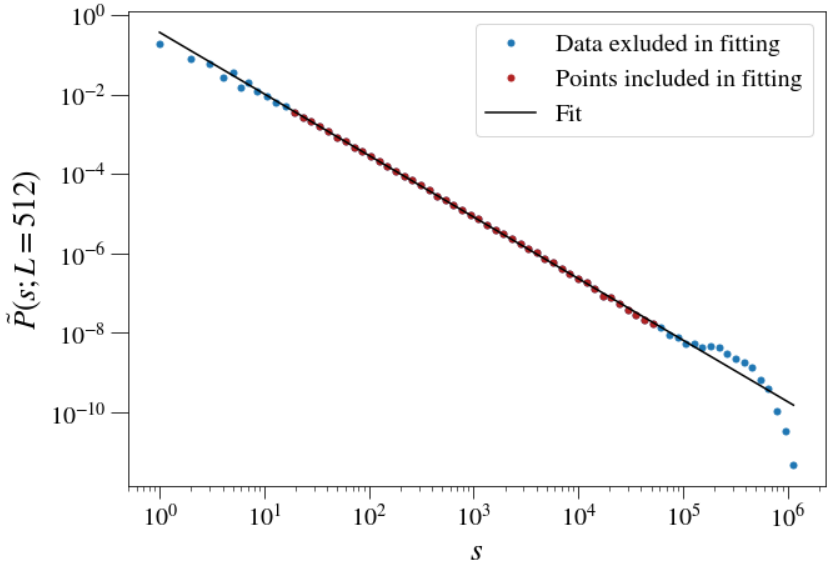

Figure 13: Log-log plot of logbinned avalanche size probability $\tilde{P}_N(s; L = 512)$ against avalanche size s for $L = 512$. The data points that are seen to lie on a linear region in the logplot were chosen to be fitted, seen in red dots here, while the blue dot data were excluded as they are not following the powerlaw.

By subsequently varying the value of D until the 'peaks' of the graph aligned, the value $D \approx 2.2 \pm 0.3$ was estimated, the large uncertainty arising from the inherent subjectivity of estimating the goodness of the collapse by eye. The convincingly good data collapse with the approximate values is seen in figure 14, acting as verification of the FSS ansatz.

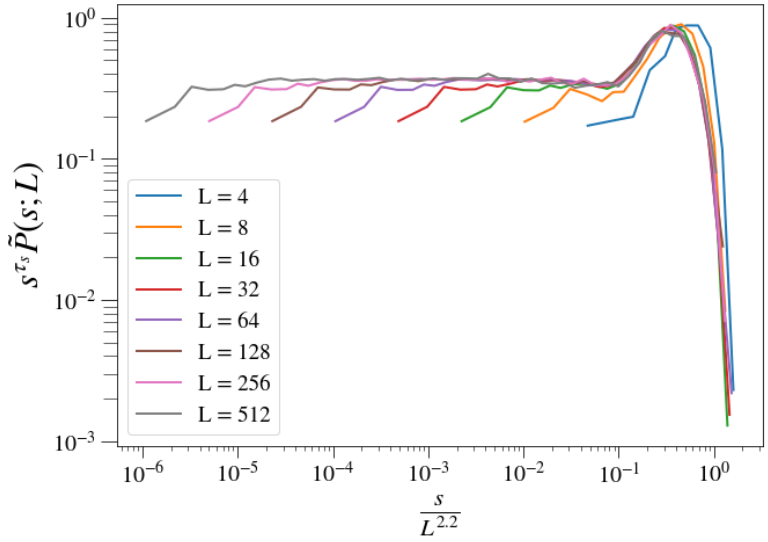

Figure 14: Log-log plot of data collapse of rescaled log-binned avalanche probability density against rescaled avalanche size using the estimates values of $D = 2.2, \tau_s = 1.55$. The goodness of fit seems fairly convincing as the distinctive feature of cut-off avalanche size seem to overlap. The smaller size pile $L = 4$ (blue line) seems to disagree the most, attributing to its large correction to scaling for the value of D.

3.2 Moment Analysis of Avalanche Size

A more accurate way to extract the values of D and τ_c is through the k'th moment analysis of the avalanche sizes. The k'th moment of the avalanche size $\langle s^k \rangle$ for $k \in \mathbb{N}$ is given by

$$\langle s^k \rangle = \lim_{T \to \infty} \frac{1}{T} \sum_{t=t_0+1}^{t_0+T} s_t^k = \sum_{s=1}^{\infty} s^k P(s; L) \tag{7}$$

where s_t is the measured avalanche size at time t and $t_0 > t_c(L)$ where t_c is the cross-over time, to ensure that the system is in steady state. A value of $t_0 = L^2$ was chosen as it is the upper bound of τ_c. Inserting the expression for the finite-scaling ansatz of equation 6 into equation 7, approximating the sum as an integral and evaluating can be shown [3] to lead to the scaling

$$\langle s^k \rangle \propto L^{D(1+k-\tau_s)} \tag{8}$$

Taking the log of equation 8 and recasting into the form

$$\log \langle s^k \rangle = D\,(1 + k - \tau_s) \log L + \log(\text{ constant }) \tag{9}$$

allowed to obtain the values of $D\,(1 + k - \tau_s)$ by measuring the gradient of the plot $\log \langle s \rangle$ against $\log L$, seen in figure 15.

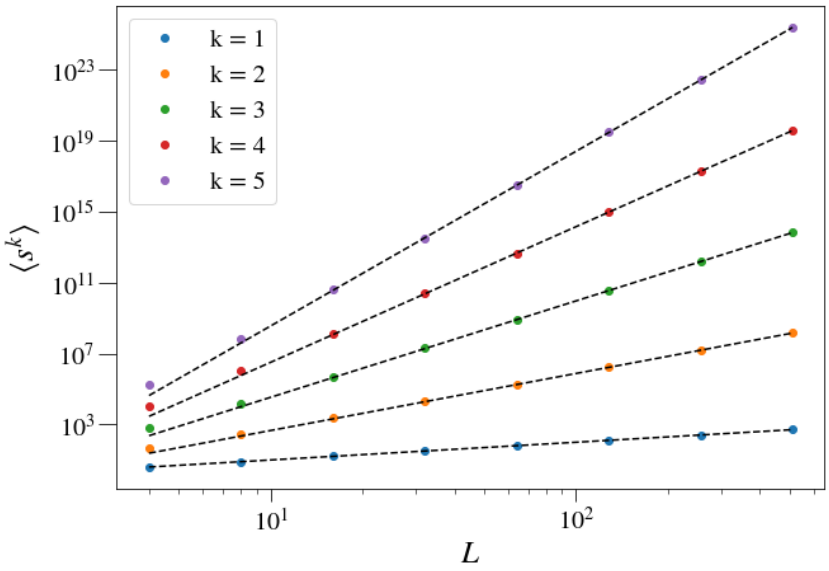

Figure 15: Log-log plot of kth avalanche-size moment against system size for $L \in \{4, 8, 16, 32, 64, 128, 256, 512\}$ (dots) and $k \in \{1, 2, 3, 4, 5\}$. Only the last 4 points corresponding to the 4 largest system sizes for each moment were plotted in the fit to avoid errors due to corrections to scaling. The slopes of the fits (dotted lines) were measured to get values for $D\,(1 + k - \tau_s)$.

Finally, the critical exponents D and τ_s were extracted from the plot of $D\,(1 + k - \tau_s)$ as a function of k, seen in figure 16, of which the slope is equal to D and the intercept is $D(1 - \tau_s)$, along with the covariance matrix for their error.

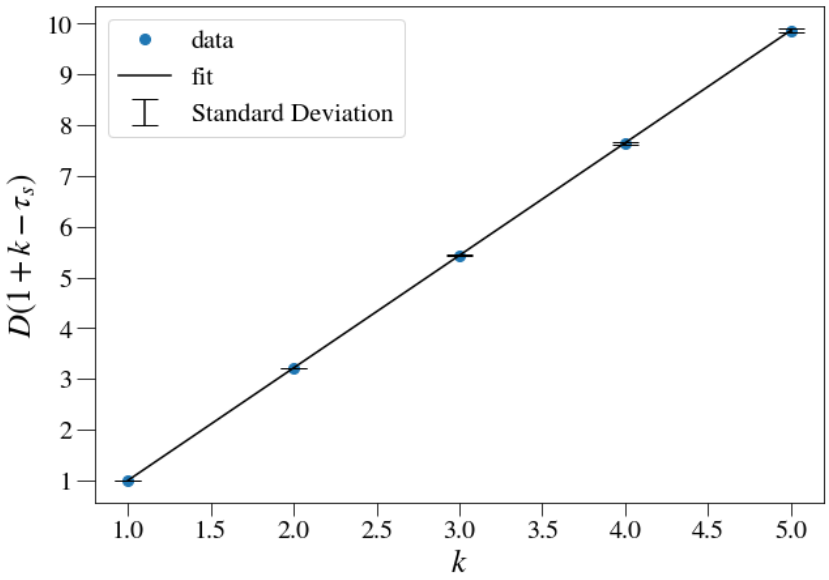

Figure 16: Log-log plot of kth avalanche-size moment against system size for $L \in \{4, 8, 16, 32, 64, 128, 256, 512\}$ (dots) and $k \in \{1, 2, 3, 4, 5\}$. Only the last 4 points corresponding to the 4 largest system sizes for each moment were plotted in the fit to avoid errors due to corrections to scaling. The slopes of the fits (dotted lines) were measured to get values for $D\,(1 + k - \tau_s)$.

The values were

$$D = 2.22 \pm 0.01$$
$$\tau_s = 1.55 \pm 0.01$$

These are in good agreement with the accepted values [3] of $D = 2.25, \tau_s = 1.55$, with the small deviations attributing to the finite system sizes considered.

A final plot of the data collapsed onto the scaling function $\mathcal{G}^{oslo}$ with the measured critical exponents is depicted in figure 17. The traced out FSS is different for each L initially but then displays universal behaviour at the characteristic bump and subsequent decay which is scale invariant as expected.

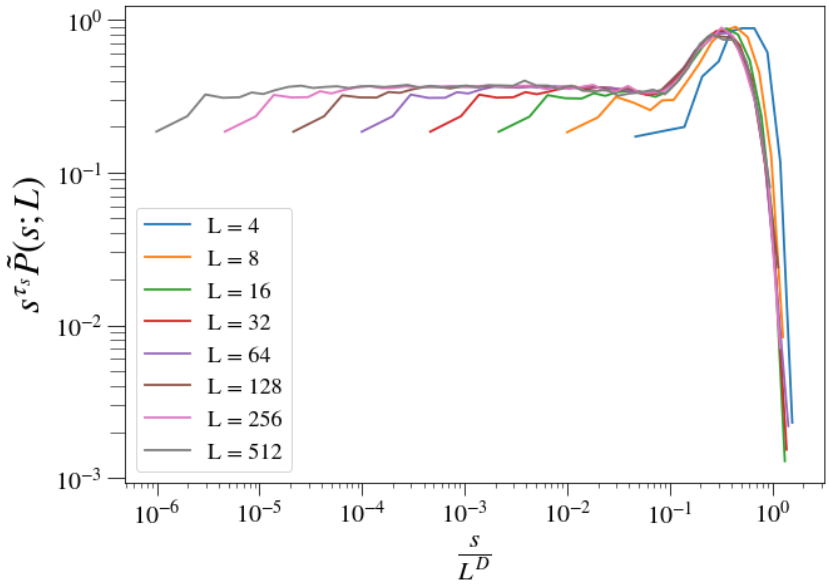

Figure 17: Data collapse onto the oslo scaling function using the obtained values of $D = 2.22$ and $\tau_s = 1.55$. As the system sizes get larger, the rescaled graphs are seen to get in greater agreement. There is a clear deviation from the collapsed function for the smaller system sizes, especially $L = 4$. This is to be expected as the corrections to scaling emerging in such small sizes are expected to be substantially high.

Conclusion

The Oslo model was computationally simulated for multiple system sizes to investigate Self-Organised Criticality. The system height was shown to enter a steady-state after the cross-over time, in which a single addition of a grain could induce an avalanche with sizes ranging several orders of magnitude. Hence, the pile was said to organise itself into a highly susceptible critical state, in which the avalanche sizes are scale invariant and are limited only by the finite system size. This behaviour was described by proposed FSS ansatzs, which were confirmed by the production of data collapses. A k'th moment analysis of the avalanche size yielded the critical size exponents $D = 2.22 \pm 0.01, \tau_s = 1.55 \pm 0.01$ which are in good agreement with the theoretical values.

References

[1] Kim Christensen, Álvaro Corral, Vidar Frette, Jens Feder, and Torstein Jøssang. Tracer dispersion in a self-organized critical system. *Physical review letters*, 77(1):107, 1996.

[2] Kim Christensen. *Complexity Project Note, Complexity and Networks Course*. Imperial College London, 2021-2022.

[3] K. Christensen and N.Maloney. *Complexity and Criticality*. Imperial College London Press, 2005.

[4] Mark Richards. *First Year Statistics of Measurement L8 Notes*. Imperial College London, 2019-2020.